8-15-2023

Spherical Harmonic analysis and filtering of Weyl Scalar ψ4

Jackson Bates

Spherical Harmonic analysis and filtering of Weyl Scalar ψ_4

by

Jackson K. Bates

A Project Submitted in Partial Fulfillment of the Requirements for the

Degree of Master of Science in Applied and Computational Mathematics

School of Mathematical Sciences, College of Science

Rochester Institute of Technology

Rochester, NY

August 15, 2023

I. Project Summary

Numerical Relativity simulations play an important role in the Astrophysics community through their ability to create templates and test specific solutions to Einstein's Field Equations. As Gravitational Wave Astronomy has grown over the past decades, the need for accurate and efficient codes has grown as well. Binary Black Hole Merger simulations provide the template needed by modern Gravitational Wave Detectors (LIGO/Virgo) to verify the integrity of detected symbols. Improvement of these merger simulations aids both the experimental and numerical sides of physics, as well as verifying the theoretical side. A major issue that arises from any numerical simulation of a dynamical spacetime related to how one can uniquely determine the radiation content. Because gravitational radiation can only be determined uniquely infinitely far from the source, current simulations use various means to *extrapolate* an approximate waveform at finite r out to $r = \infty$. In this work, we extend upon existing tools to perform this extrapolation using Cauchy-Characteristic matching (CCE). CCE uses data from a Cauchy evolution of a spacetime with radiation to generate boundary data for a second evolution, this time using Characterisitic evolution techniques, to solve for the spacetime in the vicinity of future null infinity $\mathscr{I}^+$. Here, we consider various ways of obtaining the necessary boundary data. In particular, we are interested in finding new techniques that are more robust against various sources of high-frequency numerical noise. We compare these new techniques with the original CCE algorithm, as well as purely perturbative algorithms that extrapolate the waveform at finite r to $r = \infty$ without the use of a second evolution step. Many of these newer methods perform just as accurately as their predecessor, while providing evidence towards increased efficiency in storage and computation time. Further investigation points toward the need to increase computational resolution in order to find more significant differences between these various methods.

For our study, we considered the case of two equal-mass black holes at close separation merging

into a final larger black hole. This case is well suited for standard perturbative extraction techniques, which allowed us to use the perturbative waveforms as an *exact* solution to compare to the CCE waveforms. We found that for the low-amplitude waveform modes, the numerical errors associated with poor resolution dominated the signals. While we did see see some evidence that CCE produced a lower error than the perturbative extraction techniques, because the noise dominated both signals, we could not make strong conclusions about the efficacy of CCE.

In the end, we found that a new, much more efficient, algorithm for obtaining CCE data was at least as accurate as the older techniques (while being a factor of $\sim$5 faster). With this new technique, Cauchy codes can produce CCE initial data with minimal effects on the overall runtime.

Contents

II. Introduction

Understanding Black Holes and their influence on astrophysics is an important topic in the astrophysics community. At the center of every galaxy is a region of dense matter, ranging in orders of magnitude from millions to billions of times more massive than our own sun. Radiation ranging from gamma rays up to even radio frequency is emitted from these regions. Current models of these Active Galactic Nuclei (AGN) point solely to Super Massive Black Holes as the source of these emissions. These black holes accumulate matter from the surrounding galaxy, creating luminous events that we can view from earth itself. As galaxies travel through space, they can in turn merge with one another, creating more events that lead to emissions of radiation. Understanding the mechanics that underlie all of these phenomena is essential for continuing the understanding of space-time itself. While we cannot observe black holes directly, we can still gain lots of information through how they affect the region of space around them. The motion of stellar objects and the warping of space-time itself can be observed to provide indirect evidence towards the properties of the underlying black holes they are influenced by. Before we can understand how all of these parts tie in together, we must first understand how black holes fundamentally work on their own, which requires an understanding of the General Theory of Relativity.

II.1 Einstein's theory of General Relativity

It would be beneficial to go over some basic definitions and terminology that will be used frequently within the following paper. I will give an overview of General Relativity as well as Gravitational Radiation, to lead into the more in depth topics discussed later on. Theoretically speaking, space-time can be thought of as a 4 dimensional manifold M, along with a Lorentzian metric g, which is denoted as (M, g). The metric g is a symmetric bilinear map from $T_p \otimes T_p \to \mathbf{R}$, where T_p is a tangent space of vectors. We can also expand our definition of the metric into a

system of basic vectors and covectors:

$$g = \sum_{\mu\nu} g_{\mu\nu}\, dx^{\mu} \bigotimes dx^{\nu}. \tag{1}$$

This form of the metric allows us to interchange coordinates, allowing transformations from a coordinate system x^{μ} to y^{α} through:

$$g_{\alpha\beta}(y) = \frac{dx^{\mu}}{dy^{\alpha}} \frac{dx^{\nu}}{dy^{\beta}} g_{\mu\nu}(x). \tag{2}$$

Lorentzian metrics are not positive definite, so they allow for zero length curves and vectors to exist. These null directions are essential to the theory of General Relativity. Another important note, is that a diffeomorphism mapping one spacetime (M_1, g_1) to another (M_2, g_2) means that the two spacetimes are equivalent. This one to one correspondence of spacetimes leads to a coordinate freedom in the theory, which is referred to as a gauge freedom. This ability to have corresponding spacetimes means that we cannot have a uniquely defined spacetime, thus we will need extra imposed conditions to really define what we mean. In essence, the theory itself describes how matter and spacetime are related to one another. Matter curves spacetime, and at the same time spacetime tells matter how to move. All of this is modeled through looking at local regions of spacetime, rather than from a larger macroscopic perspective. Einstein's Field Equations are given as a set of tensor equations relating spacetime curvature with energy, momentum, and stress within a system. Their general form is given by

$$G_{\mu\nu} = 8\pi T_{\mu\nu}. \tag{3}$$

where $G_{\mu\nu}$ is the Einstein Tensor and $T_{\mu\nu}$ is the stress-energy tensor. The Einstein tensor is defined in terms of the Ricci curvature tensor $R_{\mu\nu}$, the Ricci scalar R, and the metric tensor from 3;

$$R_{\mu\nu} - \frac{1}{2} R g_{\mu\nu}. \tag{4}$$

Combining 3 and 4 we get an expanded form of the field equations:

$$R_{\mu\nu} - \frac{1}{2} R g_{\mu\nu} = 8\pi T_{\mu\nu}. \tag{5}$$

Due to this relationship between spacetime and matter, there are scenarios where enough matter condensed leads to extreme curvature in the spacetime. Extreme enough that these regions cannot 'communicate' with neighboring regions of spacetime. These conditions lead us to what are known as Black Holes.

A single stationary black hole (stationary is the technical term for time independence) can be completely described by three numbers: the mass, spin, and charge of the black hole. For astrophysical scenarios, the charge is essentially zero. However, for systems of orbiting black holes, there is no known exact solution. Such a system cannot be stationary, as the black holes will attract each other. The acceleration of the black holes leads to the emission of gravitational radiation. This, in turn, leads to energy loss and an inspiral and merger. The mergers of compact objects is the primary source of observable gravitational radiation.

These regions of spacetime can be difficult to analyze, as we encounter ambiguities in coordinate systems. Gravitational waves propagate at the speed of light, so we can distinguish these ambiguities by looking at possible perturbations of the metric in the near field as they spread further from the source. We expect the spacetime in these far field regions to be essentially Minkowski (flat). A transformation/compactification of the spacetime coordinates in this regime allows for a specific definition of "far away" regions of spacetime. Here we introduce what is called Future Null Infinity $\mathscr{I}^+$. When looking at radiation that propagates out to $\mathscr{I}^+$, we have a concrete definition that what we are looking at is truly wave-fronts, rather than a side effect of gauge freedoms. This definition is based on contracting the curvature tensor with a set of 4 basis null vectors (null tetrad). The Newman Penrose (NP) formalism treats the equations of GR in terms of Spinors. These objects require 720° of rotation to "return" back to their original starting position. A single rotation of 360° will just negate the sign of the spinor. The vector basis used for this formalism is a null tetrad; made up of a real null vector pair (l^α, n^α), and a complex conjugate null vector pair ($m^\alpha, \bar{m}^\alpha$). This formalism is suited well for describing the propagation

of gravitational radiation. The Weyl Scalars $\{\psi_0, \psi_1, \psi_2, \psi_3, \psi_4\}$ contain information about the 10 independent components of the Weyl Tensor in 4D spacetime. ψ_4 in physical terms represents outgoing transverse radiation at larger distances.[1] In an asymptotically flat spacetime ψ_4 can be shown as

$$\lim_{r\to\infty} r\psi_4 = \lim_{r\to\infty} r(-\ddot{h}_+ + i\ddot{h}_\times) \tag{6}$$

where $\ddot{h}_+$ and $\ddot{h}_\times$ represent the second time derivative of plus and cross polarizations for gravitational radiation.

To understand gravitational radiation, we need to introduce the theory of weak linearized gravity. In this theory, the metric $g_{\mu\nu}$ is thought of as the Minkowski metric plus a small perturbation metric $h_{\mu\nu}$, i.e.,

$$g_{\mu\nu} = \eta_{\mu\nu} + h_{\mu\nu}, \tag{7}$$

where both the perturbation and its derivatives are small ($\|h_{\mu\nu}\| \ll 1$, $\|\partial h_{\mu\nu}\| \ll 1$).

This means that any square quantities of this perturbation metric and/or it's derivatives will essentially be zero:

$$h_{\alpha\beta}h_{\mu\nu} \approx 0,$$

$$(\partial_\gamma h_{\alpha\beta})(\partial_\sigma h_{\mu\nu}) \approx 0,$$

$$h_{\alpha\beta}(\partial_\sigma h_{\mu\nu}) \approx 0.$$

It is convenient to define h, which is the trace of $h_{\mu\nu}$ ($h = \eta^{muv}h_{\mu\nu}$), and the trace-reversed perturbation $\bar{h}_{\mu\nu} = h_{\mu\nu} - \frac{1}{2}h\eta_{\mu\nu}$. Furthermore, one can always perform a coordinate transformation such that

$$\eta^{\mu\nu}\partial_\nu \bar{h}_{\mu\sigma} = 0. \tag{8}$$

In such a gauge, the Einstein equations take on a particularly simple form

$$\partial_\mu \partial^\mu \bar{h}_{\rho\sigma} = -16\pi T_{\rho\sigma}. \tag{9}$$

For an *isolated* system, far from the source we can always find a coordinate system where the perturbation falls off as $h_{\mu\nu} = \mathcal{O}(1/r)$ and $\partial_\sigma h_{\mu\nu} = \mathcal{O}(1/r^2)$. Within this asymptotically Minkowskian gauge (i.e., a gauge where the metric approaches diag$[-1, 1, 1, 1]$), the gauge can be further refined so that the trace of $h_{\mu\nu}$ vanishes and $\partial_\mu h^{\mu\nu} = 0$. It is common to denote the metric perturbation in this transverse-traceless gauge by $h^{TT}_{\rho\sigma}$. In this gauge, the leading order contribution to h_{ab} is the radiation field itself (all other contributions arise at higher powers of $1/r$). It can be shown that $h^{TT}_{\rho\sigma}$ has two degrees of freedom. These two degrees of freedom are the h_+ and $h_\times$ discussed above.

The interpretation of h_+ and $h_\times$ as radiation fields arises from the fact that freely falling test particles will experience an apparent oscillatory tidal interaction that is directly proportional to them.

Note that constructing the transverse traceless gauge when starting from a metric in an arbitrary gauge is non-trivial.

II.2 Numerical Relativity

As the theoretical side of General Relativity grew through the early/mid 1900's, it became apparent that numerical methods would be needed to gain meaningful solutions to Einstein's Field Equations. Since the 1960's there have been advancements made to even solve for correct space-times of a single black hole. The first simulation of an orbiting binary system was done in 2005 by Frans Pretorius. [2], followed soon after this in 2006 was the Moving Puncture method which allowed for solutions of the Einstein Equations without the need for excision or a co-rotating shift. [3, 4]

From these initial breakthroughs came the Lazarus Evolution Code (LazEv), which is based on The Einstein Toolkit (ETK). ETK is an open source project useful for computational research in gravitational and relativistic astrophysics. It is composed of over 270 components called 'thorns', providing tools and computational frameworks for relativistic hydrodynamics, vacuum spacetime solvers, and other initial data problems [5]. At the time of its release in 2010, the toolkit had computing capabilities of 3D BSSN spacetime as well as the Valencia Formalism for GR Hydrodynamics. It provided an evolution code, initial data for punctures, waveform extraction and horizon solvers. Cactus was the name given to the computational framework, hence the components being named thorns. Carpet provides adaptive mesh refinement capabilities to the framework. LazEv itself is capable of simulating various useful systems in Numerical Relativity such as Binary Black Holes mergers, 3 Black hole systems, as well as extreme cases such as binaries with large separations or large differences between the binary masses. This led to RIT's gravitational waveform catalog; a useful set of templates for varying parameters in Binary Black Hole mergers. [6] The catalog contains hundreds of quasicircular wave-forms. These wave-forms covered various initial parameter setups, such as non-spinning, aligned spin, and precessing spin binaries. All of these templates are useful for real world applications; primarily to line up with actual gravitational wave detections found by LIGO; the Laser Interferometer Gravitational-Wave Observatory. [7].

LazEv, like most other numerical code, solves the Einstein Equations using a Cauchy evolution of initial/boundary data. Such a code cannot evolve the metric out to infinity (the main limitation here is that if the space is *compactified*, the coordinate wavelength of the gravitational wave will be unresolvable at large r). Characterisitic codes [8, 9, 10, 11, 12, 13, 14, 15, 16], use a different technique where the metric is evolved from outgoing lightcone to outgoing lightcone (see Fig. 1). In such a scheme, radial compatification does not affect the resolution of the waveform.

Cauchy and characteristic methods provide different routes to get gravitational radiation calcu-

lations, while having their own respective uncertainties/errors. In Cauchy schemes, the '3+1' spacetime is setup into finite spacelike hypersurfaces, with an artificial spatial boundary. Gravitational radiation in the form of waves can have reflective patterns at this outer boundary. Cauchy code typically calculate the gravitational waveform by calculating ψ_4 on spatial slices and extrapolating to $r = \infty$. This technique is accurate in the perturbative regime, but has known (although small) errors associated with it [17].

Cauchy Characteristic Extraction (CCE) is the technique of using data from a Cauchy evolution to provide the inner boundary data for a characteristic evolution. There is no feedback from the Characteristic evolution to the Cauchy evolution (if a feedback mechanism is provided, then this is referred to as Cauchy-Characteristic-Matching, but no current NR code performs this yet). CCM would provide a convergent approximation to the true analytical solutions given a of set initial conditions [8]. While these methods have been proven to work in various relativistic situations, they still come with their own sources of uncertainty. Boundary conditions play an important role in this uncertainty, as much of the computational framework revolves around matching data from regions of spacetime that are mathematically separated in this configuration.

III. Objectives

The accuracy and efficiency of algorithms within Numerical Relativity is a high priority, as high resolution simulations of BBH mergers can take weeks if not months to get sufficient progress. The LazEv simulations that are used to supply initial data for gravitational wave extraction techniques such as CCE have issues at the boundaries. Low amplitude, high frequency noise is introduced through these initial LazEv runs due to the caustic issues. From this the data fed into CCE has an imprint of this noise, which can be easily seen in the wave-forms generated from the extraction. The primary objective of this project is to explore various computational methods that help to resolve the noise in generated wave-forms. In addition, I will explore the accuracy and efficiency

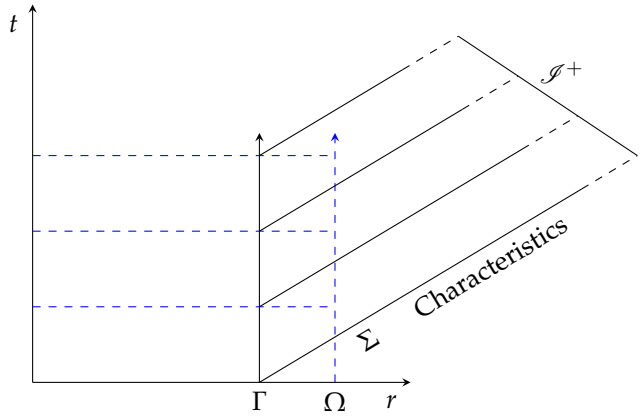

Figure 1: Visualization of Cauchy Characteristic Extraction in regards to the t and r axis (θ and ϕ not shown). The Cauchy slices with their outer boundary Ω are shown in blue. CCE data is provided on the worldtube Γ, while initial data for the characteristic evolution is provided on the initial characteristic slice Σ. Γ lies inside of Ω This data is then propagated out to $\mathscr{I}^+$ through the extraction algorithm.

of these methods. Various ways of decomposing data allow for filtering of the noise, as well as reducing the computational cost of simulating Binary Black Hole Mergers.

Our goal here is to develop methods that generalized across numerical frameworks to extract the metric data from a Cartesian Cauchy AMR simulation to generate boundary data for CCE. To this end, we will explore different extraction techniques, paying careful attention to numerical errors and computational costs. Our goal is to make the extraction part of CCE both accurate and computationally inexpensive.

Fundamentally, at each time slice, we need to obtain the metric and all of its first derivatives (radial, angular, time) on a sphere and store that data. One major complication is that the metric data is *noisy*. This stochastic noise [18] is enhanced by CCE, leading to larger high-frequency errors in the CCE waveform than in the original Cauchy data.

IV. Methods

We started this project using the original CCE extraction code from the Einstein Toolkit [14]. That code decomposed the metric on a spherical shell in terms of a Chebyshev radial basis (using Chebyshev polynomials of the second type) and a spherical harmonic radial basis. For both bases, the actual coefficients were constructed by interpolating the metric data on a set of equally spaced points in radius, $\cos(\theta)$ and ϕ (θ, ϕ being the usual polar and azimuthal angles on the sphere) and then performing a least-squares fit. In the sections below, we will refer to this original technique as LS.

We explored several modifications to this procedure. First, we used the Driscol-Healy algorithm [19] to decompose the metric data on the sphere in terms of a *small* number of spherical harmonics. Second, we used the discrete orthogonality of the Chebyshev polynomials of the first kind in order to construct the radial modes. Finally, we removed the radial decomposition entirely and instead extracted both the metric and its radial derivative on a single sphere.

The end result in each case is a time series of the relevant spectral coefficients. This time series in general lacks differentiability in time, which results in a high-frequency *flip-flop* mode apparent in the higher-order modes of the waveform. We reduce the effects of this by filtering the data through an bandwidth limited FFT. Note that this high-frquency noise, and its FFT mitigate, were discussed in [14]

We describe these numerical methods below.

Spherical Harmonics: Given a set of angular coordinates (θ, ϕ), the Spherical Harmonics provide an orthonormal basis for functions on the surface of a sphere. This is analogous to the Fourier Series for a periodic function on a circle. Spherical harmonic functions are defined with a degree l and order m:

$$Y_l^m(\theta, \phi) := N_{lm} e^{im\varphi} P_l^m(cos(\theta)), \tag{10}$$

where P_l^m is the associated Legendre polynomial

$$P_l^m(x) : (-1)^m (1-x^2)^{\frac{m}{2}} \frac{d^m}{dx^m}(P_l(x)), \tag{11}$$

and P_l is the ordinary Legendre polynomial (expressed using Rodrigues' formula)

$$P_l(x) : \frac{1}{2^l l!} \frac{d^l}{dx^l}(x^2-1)^l. \tag{12}$$

Chebyshev Polynomials for radial points When extracting each grid-function for CCE, we decompose the signal into both radial and angular modes. For the radial modes, originally we used the Chebyshev Polynomials of the second kind $U_n(x)$, however these polynomials do not obey a discrete orthogonality relationship over the entire basis. Due to this we chose to use the Chebyshev Polynomials of the first kind $T_n(x)$, which provide orthogonality for all N Chebyshev modes; (if N is the size of the basis):

$$T_n(x) = \cos(n \arccos x) \tag{13}$$

$$U_0(x) = 1 \tag{14}$$

$$U_1(x) = 2x \tag{15}$$

$$U_n(x) = 2xU_{n-1}(x) - U_{n-2}(x). \tag{16}$$

It was also more efficient using the first kind polynomials, as they have an explicit trigonometric definition. Here we are using the case of $|x| < 1$, since that is one of the conditions set on our radial points already. Previously we had explicitly defined every second kind polynomial up to the expected number of modes. Now we just have a single definition that can be used for any value of n. The main focus of these methods is to obtain coefficient values for the Spherical Harmonics. Data is given to these methods in the form of grid-function values over a collection of (θ, φ) points, as well as over multiple spherical shells varying in radius. Obtaining these coefficient

values accurately and efficiently is a main priority. A comparison of these methods is detailed further in the Results section. (V)

Least Squares Fitting: Given a set of points $x = \{(\theta_1, \varphi_1), \ldots, (\theta_m, \varphi_m)\}$ and the ordered Spherical Harmonic functions $Y_l^m = \{Y_0^0, Y_1^{-1}, Y_1^0, Y_1^1, \ldots Y_6^6, \}$ (for $l_{max} = 6$) we can construct a linear system of equations that can be solved using least squares fitting. In our CCE simulations, we end up with function values B_i at each specific point x_i in our grid. These function values can be thought of as a summation of every Y_l^m mode (that we care about) at this specific location:

$$B_i = \sum_{\substack{l=0\ldots6 \\ m=-l\ldots l}} C_l^m Y_l^m(x_i. \tag{17}$$

The C_l^m coefficients within the summation are what we want to obtain through these methods, they represent the actual amplitude of the Spherical Harmonic basis functions that we care about. If we were to look at every function value B_i relative to it's equivalent basis form, we come to our system of equations for C_l^m, relative to a predicted value for B_i which I am labeling P_i here:

$$\begin{bmatrix} Y_0^0(x_1) & Y_1^{-1}(x_1) & \ldots & Y_6^5(x_1) & Y_6^6(x_1) \\ Y_0^0(x_2) & Y_1^{-1}(x_2) & \ldots & Y_6^5(x_2) & Y_6^6(x_2) \\ \vdots & \vdots & \ddots & \vdots & \vdots \\ Y_0^0(x_{m-1}) & Y_1^{-1}(x_{m-1}) & \ldots & Y_6^5(x_{m-1}) & Y_6^6(x_{m-1}) \\ Y_0^0(x_m) & Y_1^{-1}(x_m) & \ldots & Y_6^5(x_m) & Y_6^6(x_m) \end{bmatrix} \begin{bmatrix} C_0^0 \\ C_1^{-1} \\ \vdots \\ C_6^5 \\ C_6^6 \end{bmatrix} = \begin{bmatrix} P_1 \\ P_2 \\ \vdots \\ P_{m-1} \\ P_m \end{bmatrix}.$$

Given the above system, we are then able to approximate the values of C_l^m through Least Squares fitting. In this case, we would have a minimization problem. Here we are trying to minimize a squared difference χ^2 given our predicted coefficients P_i:

$$\chi^2 = \sum_i (P_i - B_i)^2 . \tag{18}$$

Driscol-Healy: In an updated method for coefficient solving, we turn towards using FFT's as well as an integral equation that was developed by Driscol and Healy [19] For this scenario, we again

look at the grid-function values B_i at each location point, except here we make a distinction of looking at the points in a 2-dimensional view, rather than the 1-d flattened view as in the Least Squares fitting case. I find it better to denote these data points B_θ^φ in this case. Given our 2-d matrix of function values at point pairs, we then will compute the FFT of this data only in the φ direction. At this point we now have data that represents normal θ based information, and FFT modes in the φ direction; B_θ^m (where m represents the Fourier mode in the phi direction). From here, we find each Spherical Harmonic coefficient through a summation equation:

$$C_l^m = \sum_\theta B_\theta^m \, W_i \, sin(\theta_i) \, d\theta. \tag{19}$$

Where W_i are the Driscol-Healy weights associated with this algorithm:

$$W_i = \frac{4}{\pi} \sum_{l=0}^{\frac{n_\theta}{2}-1} \left(\frac{sin((2l+1)\theta_i)}{2l+1} \right). \tag{20}$$

Filtering in time with FFT: Originally in the SphericalHarmonicDecmomp directory there was an FFT based program that filtered along the time dimension called fftwfilter. The hdf5 (Hierarchical Data Format) utilities within C were less verbose and required much more under-the-hood knowledge. To avoid future conflicts and improve readability, a Python3 version of the C code was created. This allowed for much quicker updates to the filtering functionality as we changed how the metric files were created and formatted. While Python is known for one of the quicker interpreted languages, we did notice that filtering took roughly twice as long as before to finish. Most of the issues fell back to the h5py library, with aims to recreate the hd5f functionally in Python. Reading and writing the data sets themselves was the biggest drawback in speed, compared to the actual filtering transformations themselves. For Fourier modes $i = 1 \ldots \lfloor n_{max}/2 \rfloor + 1$

$$f(x) = \frac{1}{2} \left[1 + erf(\sigma(i - k_{max})) \right] \tag{21}$$

gives the filtering function for the data.

V. Results

V.1 Preliminary Python Tests

To initially test the effectiveness of methods described in Section IV, a Python3 Jupyter notebook was developed to compare accuracy and noise reduction between the Least Squares and Driscol-Healy algorithms. Jupyter allows for a higher level of debugging and reuse for python scripts as separate lines of code can be ran out of their normal order of operations. In both tests we sampled a test function (composed of already known Spherical Harmonics) over a set of (θ_i, φ_i) points for $\theta_i \in [0, \pi]$, $\varphi_i \in [0, 2\pi]$. Tests were done with an input signal B_i consisting of a sum of Y_l^m modes decreasing in amplitude as l and m get larger, up to a maximum of $l = 6, m = 6$. Uniform random noise was added into this signal at an order of 0.1% relative to our input signal amplitude. Noise-free tests were done initially to verify the algorithm was implemented correctly, with errors on the order of 10^{-15} when solving for the original function values in both cases. In the Least Squares case, the points were evenly spaced. However the Driscol-Healy case requires that the theta points are staggered on both endpoints by a factor of $\Delta\theta$ relative to the number of theta points. The endpoint of 2π is also excluded for the phi points. Both of these conditions resolve issues with the poles in this algorithm.

V.1.1 Comparing Least Squares and Driscol-Healy

In an effort to compare and contrast these two methods, I ran scaling tests varying the amount of points in theta and phi used to sample our input functions. These scaling tests compared the input sources B_i with the found solutions S_i of both algorithms, which ideally would effectively get rid of the random uniform noise that was introduced to the input signal. Here I used the L^∞ norm relative to these input and solution vectors; $max(|B_i - S_i|)$ as my error norm.

Even though these are fabricated tests, they seem to definitely point in the direction that the

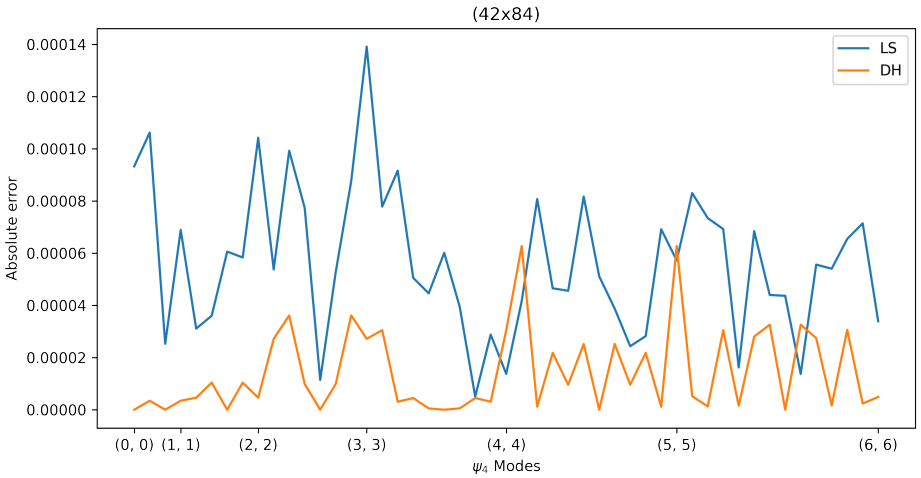

Figure 2: A comparison of the error in the reconstructed spherical harmonic coefficient from noisy data. The mode number of the coefficient is given on the x-axis. Here the blue curve shows the error obtained using the original least-squares method proposed in [14], while the orange curves shows the errors obtained using the new Driscol-Healy algorithm. A clear reduction in the effect of the noise is apparent.

Driscol-Healy algorithm seems to be advantageous in terms of accuracy. As well as accuracy, I even timed the scaling tests for each method, and Driscol-Healy was on average about twice as fast as the Least Squares fitting. As well as scaling tests, I took a look specifically at the $(N_\theta, N_\phi) = (42, 84)$ test in regards to error relative to the recovered Y_l^m coefficient. In Fig. 2, we show the error in the recovered coefficients for the different modes for the new Driscol-Healy algorithm and the original least-squares algorithm. For this test, we see a clear reduction in the error for the Driscol Healy algorithm. In Fig. 3, we compare the largest error in the recovery of the coefficients versus the number of points in theta for the two algorithms. The Driscol-Healy algorithm is superior if the number of theta points is between 15 and 100 (typical values used are ~ 45).

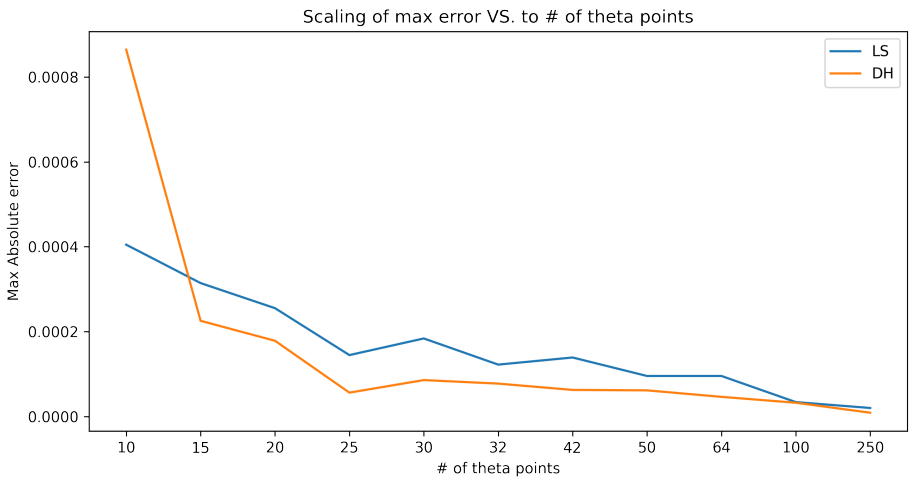

Figure 3: A comparison of the error in the reconstructed spherical harmonic coefficient from noisy data. Here we plot the maximum error (over all recovered modes) versus the number of θ points. Here the blue curve shows the error obtained using the original least-squares method proposed in [14], while the orange curves shows the errors obtained using the new Driscol-Healy algorithm. With the exception of very-high numbers of θ points, the new algorithm outperforms the original.

V.2 CCE Results

A large portion of the CCE results were generated from Lazev runs with a setup of $q = 1$ (i.e., equal masses), $\chi = 0.4$ (i.e., spins at 40% of the maximum allowed) and an initial separation of $d = 5M$. These data sets were evolved using the LazEv code and different techniques were used to extract the appropriate worldtube data for the subsequent CCE simulations. The original method for generating CCE used Least Squares fitting to obtain both the Spherical Harmonic Decomposition and the Chebyshev (using Chebyshev polynomials of the second kind) radial decomposition. From there we updated the Chebyshev basis to the Chebyshev T polynomials instead of the U. The Chebyshev T basis satisfies a simple discrete orthogonality condition. We used this condition, rather than Least-Squares fitting to obtain the radial coefficients. To obtain the spherical harmonic decomposition, we used the integration methods developed by Driscol and Healy. The radial decomposition is actually used in CCE to obtain the radial derivatives of the metric functions on the extraction worldtube. A natural question then is, could these radial derivatives be obtained directly from the Cauchy code? We compare algorithms that use a full 3D decomposition (in r,θ,ϕ) of the metric in finite spherical shell to algorithms that use a 2D decomposition the metric and its radial derivative on a fixed sphere. In the figures below, we distinguish between these two different types of decomposition by appending either 3D or 2D the legends.

In Figs. 4 and Fig. 5 we compare the the $(\ell = 2, m = 2)$ and $(\ell = 4, m = 4)$ modes of the CCE waveform obtained using the original algorithm, the new Driscol-Healy + Chebyshev T algorithm, and Driscol Healy algorithm applied to both the metric and its radial derivative. We use FFT filtering in time on all the CCE data except the one labeled as unfiltered. From the perspective of looking at the entire waveform, there seems to be no major differences between the two methods in terms of the waveform accuracy. As well as this, there were comparisons made between

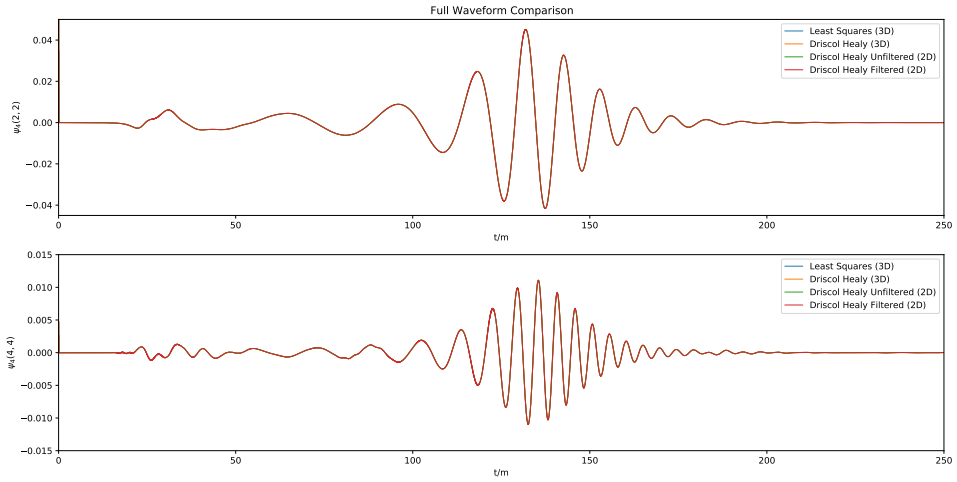

Figure 4: A comparison between the full $\psi_4(2,2)$ and $\psi_4(4,4)$ wave forms, showing that the different methods agree on the macroscopic level aside from a slight misalignment for the Least Squares method in the ring down region of the wave.

FFT-filtered and unfiltered Decomposition for the Spherical Harmonics. For both the filtered and unfiltered runs, we moved away from the Chebyshev decomposition in r, and instead directly computed the radial components and derivatives from the Spherical Harmonics themselves. A full plot of all four compared together is shown below in Fig. 4. As we can see, there isn't a significant difference in the wave-forms from a distance, it's only when we look at specific parts of the signal in detail that we notice variations. I focused on three specific locations within the waveform to identify these variations; early noise due to Lazev, the largest peak at merger, and then finally the ring-down towards the end of the signal. Once we look more carefully at each of these spots, we can see some interesting differences between all 4 data sets. Differences between the signals were more pronounced for the $\psi_4(4,4)$ mode, especially noticeable during the initial parts of the signal, as seen in Fig. 5 Even with the erratic jumping noticeable in the unfiltered radial case, it seems to be a much better overall fit in terms of the trend of the signal; which can be seen directly through

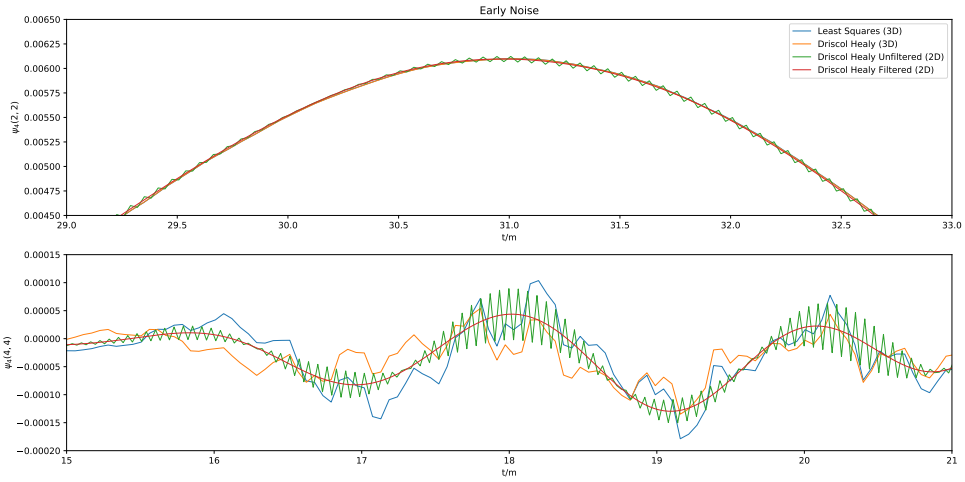

Figure 5: Comparisons of the initial junk radiation within $\psi_4(2,2)$ and $\psi_4(4,4)$. While the only noticeable difference within $\psi_4(2,2)$ is the unfiltered (Time FFT) data, the differences between all 4 methods are exaggerated within the $\psi_4(4,4)$ comparison.

the filtered radial signal. Comparatively to the older Least Squares/Chebyshev case, the newer runs seem to have a better time smoothing out the initial noise generated by Lazev. The $\psi_4(2,2)$ signal only shows some slight differences at the largest peak of the initial noise, and even then the only major difference is the back and forth jumping of the unfiltered signal. Clearly the FFT filtering in angular modes is very beneficial for these simulation. For the peak of the merger, we start to notice where the direct radial signal differs from the older Chebyshev decomposition. Both the Least Squares and Driscol-Healy with Chebyshev decomposition have amplitude differences, as well as perhaps a shift in phase, although there is not enough evidence to definitely say that it is a phase difference. For the ring-down, there are similar variations in the signals when compared to the merger. The amplitude and possible phase differences are apparent again between the old and newer radial changes: It is interesting to note that the $\psi_4(2,2)$ signal has a very apparent difference with the original least squares signal. While there seemed to be no significant differences during

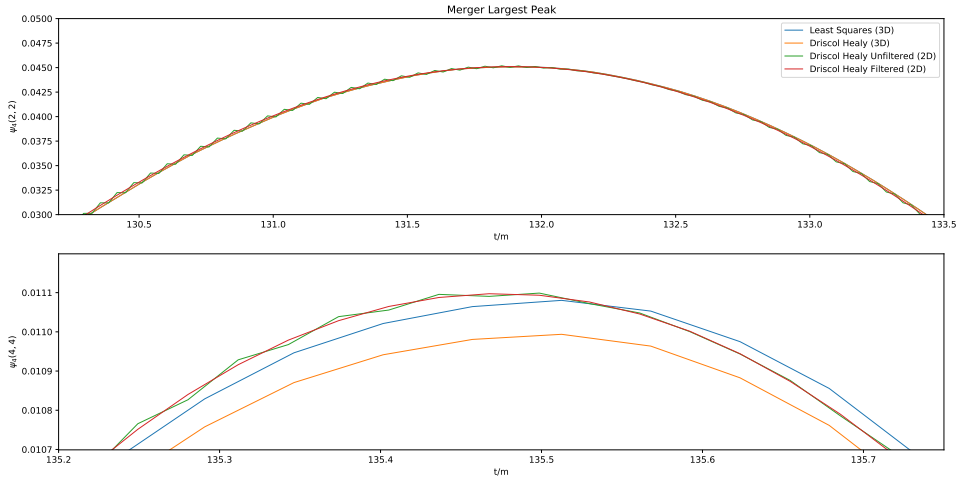

Figure 6: A view of the largest peak during merger between $\psi_4(2,2)$ and $\psi_4(4,4)$. While the differences in amplitude here are minor compared to the overall size of the wave, there still appears to be a noticeable difference between the older Chebyshev based radial decompositions and the new direct methods.

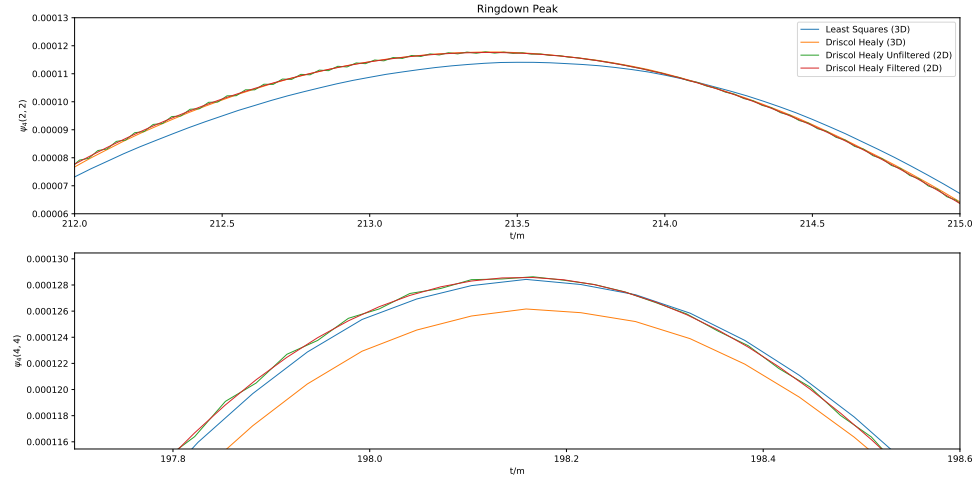

the merger, there is enough of a difference by the end of the signal. Also to note is the fact that the Driscol-Healy signal with the older Chebyshev decomposition seems to line up with the newer direct radial signal. Aside from the amplitude differences in $\psi_4(4,4)$ throughout the initial and merger parts of the signal, this seems to be a part of the wave-form where the Least squares is singled out, and the radial change is not shown to be the significant differentiator.

In certain low frequency modes such as the $(2,0)$ and $(4,0)$, we found some key differences between the various CCE methods and the Cauchy code results that were fed into CCE. Extrapolated/Rescaled waveform data from the Cauchy code seemed to deviate from the overall CCE waveform pattern later on in the signal. As well as this, the Extrapolated data in both $(2,0)$ and $(4,0)$ appears to not converge towards 0 (see Fig. 7). While both the CCE and Cauchy signals in these modes contained numerical noise, it appears that we can at least conclude that the CCE and Rescaled waveforms make more sense if we are worrying about further implications from a ψ_4 signal that does not decay over time.

We conclude by noting that storing the data from the Chebyshev radial decomposition consumes a factor of about 10 times more disk space than the decomposition of the radial derivatives. This cost is entirely due to the number of radial points required for the former algorithm. In total $N_{\text{fields}} \times N \times N_{\text{ang}}$ coefficients need to be stored for the former method. For the latter, only $2 \times N_{\text{fields}} \times N_{\text{ang}}$ coefficients need to be stored.

VI. Conclusion

Each of the methods described previously led to wave-form calculations that in a general sense 'fit' the expected profile. It was only when we look closely at these wave-forms that we notice significant differences. The initial change of the Chebyshev basis from $U(x)$ to $T(x)$ provided the same accuracy results, while providing an easier way to generate the basis, as the functions $T(x)$ can be computed individually as needed, instead of hard coding each $U(x)$ polynomial, or

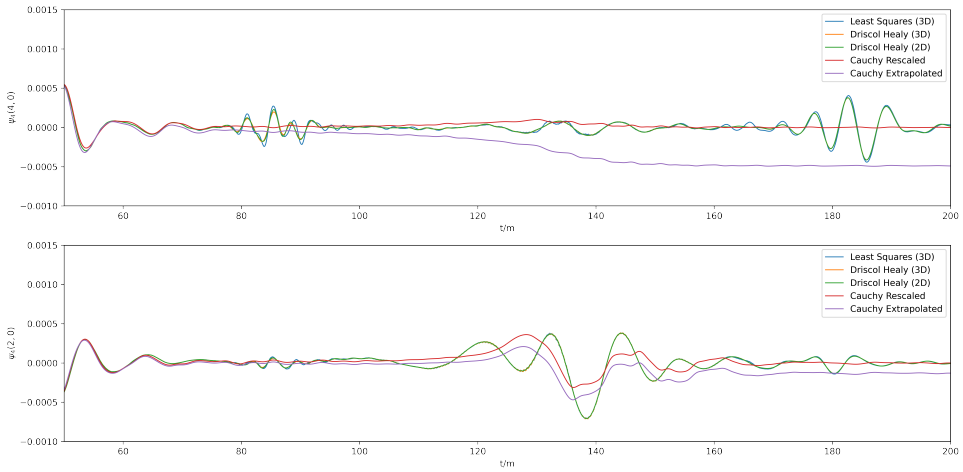

Figure 7: A comparison between the various CCE methods with results from the Extrapolated and Rescaled Cauchy waveforms. While all of the signals present are contaminated with numerical noise, it is evident that the extrapolated Cauchy data does not seem physically valid. The data in both of these low frequency modes for the extrapolated case would imply that an infinite amount of energy was radiated away from the Binary Merger, which can't be true based our current understanding of physics.

having to come up with a recursive definition within the code. When switching entirely away from the Chebyshev basis to direct radial computations, initial noise in the waveform is almost entirely removed. It is important to note that the newer direct radial computations led to increased "jumping" in the data, however with correct FFT filtering, we arrived at a wave-form that removed the initial junk noise, as well as the extra 'noise' introduced with this new method. The beginning parts of the wave-forms showed the largest deviations, while later parts (merger and ringdown) only had slight amplitude/phase differences. From an initial testing standpoint, it appears that the Driscol-Healy decomposition for Y_l^m is superior. While there were initial tests (Driscol-Healy with old Chebyshev basis) that contained the initial noise comparable to Least-Squares, the introduction of the direct radial computation was by far the best choice along with Driscol-Healy. From a computational efficiency standpoint, the direct radial computation is superior in that you no longer need to account for a radial basis of points, the entire radial decomposition methods are replaced with a faster, more direct method. Overall the suggested route going forward would be Driscol-Healy decomposition in angular coordinates, direct radial component computations from Y_l^m paired with the FFT filtering to get rid of extra noise introduced. The future of these methods can be explored by implementing them into newer computational systems. The Dendro-GR system is a primary candidate for testing going forward. Dendro is a Numerical Relativity toolkit similar to the Einstein Toolkit, however it has newer computational tools and methods; specifically octree based adaptive mesh refinement (AMR). [20] Conversion of the CCE algorithm from ETK to Dendro would be the next step in advancing the possibilities of these methods. The coupling of AMR with the already efficient CCE algorithms could lead to much quicker total simulation times. Currently higher resolution simulations can take weeks if not months to complete. Increased efficiency of these simulations through AMR would be beneficial for the Numerical Relativity community in terms of the amount of analysis able to be done in less time. As well as this, we may be able to explore new/extreme cases of Binary Black hole mergers that were previously

unatainable due to computational limitations.

VII. Bibliography

References

[1] P. Szekeres, "The Gravitational compass," *J. Math. Phys.*, vol. 6, pp. 1387–1391, 1965.

[2] F. Pretorius, "Evolution of binary black hole spacetimes," *Phys. Rev. Lett.*, vol. 95, p. 121101, 2005, gr-qc/0507014.

[3] M. Campanelli, C. O. Lousto, P. Marronetti, and Y. Zlochower, "Accurate evolutions of orbiting black-hole binaries without excision," *Phys. Rev. Lett.*, vol. 96, p. 111101, 2006, arXiv:gr-qc/0511048.

[4] J. G. Baker, J. Centrella, D.-I. Choi, M. Koppitz, and J. van Meter, "Gravitational wave extraction from an inspiraling configuration of merging black holes," *Phys. Rev. Lett.*, vol. 96, p. 111102, 2006, gr-qc/0511103.

[5] R. Haas, C.-H. Cheng, P. Diener, Z. Etienne, G. Ficarra, T. Ikeda, H. Kalyanaraman, N. Kuo, L. Leung, C. Tian, B.-J. J. Tsao, A. Wen, M. Alcubierre, D. Alic, G. Allen, M. Ansorg, F. G. L. Armengol, M. Babiuc-Hamilton, L. Baiotti, W. Benger, E. Bentivegna, S. Bernuzzi, T. Bode, G. Bozzola, S. R. Brandt, B. Brendal, B. Bruegmann, M. Campanelli, F. Cipolletta, G. Corvino, S. Cupp, R. D. Pietri, H. Dimmelmeier, R. Dooley, N. Dorband, M. Elley, Y. E. Khamra, J. Faber, T. Font, J. Frieben, B. Giacomazzo, T. Goodale, C. Gundlach, I. Hawke, S. Hawley, I. Hinder, E. A. Huerta, S. Husa, S. Iyer, L. Ji, D. Johnson, A. V. Joshi, W. Kastaun, T. Kellermann, A. Knapp, M. Koppitz, P. Laguna, G. Lanferman, F. Löffler, H. Macpherson, J. Masso, L. Menger, A. Merzky, J. M. Miller, M. Miller, P. Moesta, P. Montero, B. Mundim, P. Nelson, A. Nerozzi, S. C. Noble, C. Ott, R. Paruchuri, D. Pollney, D. Radice, T. Radke, C. Reisswig, L. Rezzolla, D. Rideout, M. Ripeanu, L. Sala, J. A. Schewtschenko, E. Schnetter, B. Schutz, E. Seidel, E. Seidel, J. Shalf, K. Sible, U. Sperhake, N. Stergioulas, W.-M. Suen, B. Szilagyi,

R. Takahashi, M. Thomas, J. Thornburg, M. Tobias, A. Tonita, P. Walker, M.-B. Wan, B. Wardell, L. Werneck, H. Witek, M. Zilhão, B. Zink, and Y. Zlochower, "The einstein toolkit," Oct. 2022. To find out more, visit http://einsteintoolkit.org.

[6] "Ccrg@rit catalog of numerical simulations."

[7] B. P. Abbott, R. Abbott, R. Adhikari, P. Ajith, B. Allen, G. Allen, R. S. Amin, S. B. Anderson, W. G. Anderson, M. A. Arain, M. Araya, H. Armandula, P. Armor, Y. Aso, S. Aston, P. Aufmuth, C. Aulbert, S. Babak, P. Baker, S. Ballmer, C. Barker, D. Barker, B. Barr, P. Barriga, L. Barsotti, M. A. Barton, I. Bartos, R. Bassiri, M. Bastarrika, B. Behnke, M. Benacquista, J. Betzwieser, P. T. Beyersdorf, I. A. Bilenko, G. Billingsley, R. Biswas, E. Black, J. K. Blackburn, L. Blackburn, D. Blair, B. Bland, T. P. Bodiya, L. Bogue, R. Bork, V. Boschi, S. Bose, P. R. Brady, V. B. Braginsky, J. E. Brau, D. O. Bridges, M. Brinkmann, A. F. Brooks, D. A. Brown, A. Brummit, G. Brunet, A. Bullington, A. Buonanno, O. Burmeister, R. L. Byer, L. Cadonati, J. B. Camp, J. Cannizzo, K. C. Cannon, J. Cao, L. Cardenas, S. Caride, G. Castaldi, S. Caudill, M. Cavaglià , C. Cepeda, T. Chalermsongsak, E. Chalkley, P. Charlton, S. Chatterji, S. Chelkowski, Y. Chen, N. Christensen, C. T. Y. Chung, D. Clark, J. Clark, J. H. Clayton, T. Cokelaer, C. N. Colacino, R. Conte, D. Cook, T. R. C. Corbitt, N. Cornish, D. Coward, D. C. Coyne, J. D. E. Creighton, T. D. Creighton, A. M. Cruise, R. M. Culter, A. Cumming, L. Cunningham, S. L. Danilishin, K. Danzmann, B. Daudert, G. Davies, E. J. Daw, D. DeBra, J. Degallaix, V. Dergachev, S. Desai, R. DeSalvo, S. Dhurandhar, M. Díaz, A. Dietz, F. Donovan, K. L. Dooley, E. E. Doomes, R. W. P. Drever, J. Dueck, I. Duke, J.-C. Dumas, J. G. Dwyer, C. Echols, M. Edgar, A. Effler, P. Ehrens, E. Espinoza, T. Etzel, M. Evans, T. Evans, S. Fairhurst, Y. Faltas, Y. Fan, D. Fazi, H. Fehrmenn, L. S. Finn, K. Flasch, S. Foley, C. Forrest, N. Fotopoulos, A. Franzen, M. Frede, M. Frei, Z. Frei, A. Freise, R. Frey, T. Fricke, P. Fritschel, V. V. Frolov, M. Fyffe, V. Galdi, J. A. Garofoli, I. Gholami, J. A. Giaime, S. Giampanis, K. D. Giardina, K. Goda, E. Goetz, L. M. Goggin, G. González, M. L. Gorodetsky, S. Goßler, R. Gouaty, A. Grant, S. Gras, C. Gray, M. Gray, R. J. S.

Greenhalgh, A. M. Gretarsson, F. Grimaldi, R. Grosso, H. Grote, S. Grunewald, M. Guenther, E. K. Gustafson, R. Gustafson, B. Hage, J. M. Hallam, D. Hammer, G. D. Hammond, C. Hanna, J. Hanson, J. Harms, G. M. Harry, I. W. Harry, E. D. Harstad, K. Haughian, K. Hayama, J. Heefner, I. S. Heng, A. Heptonstall, M. Hewitson, S. Hild, E. Hirose, D. Hoak, K. A. Hodge, K. Holt, D. J. Hosken, J. Hough, D. Hoyland, B. Hughey, S. H. Huttner, D. R. Ingram, T. Isogai, M. Ito, A. Ivanov, B. Johnson, W. W. Johnson, D. I. Jones, G. Jones, R. Jones, L. Ju, P. Kalmus, V. Kalogera, S. Kandhasamy, J. Kanner, D. Kasprzyk, E. Katsavounidis, K. Kawabe, S. Kawamura, F. Kawazoe, W. Kells, D. G. Keppel, A. Khalaidovski, F. Y. Khalili, R. Khan, E. Khazanov, P. King, J. S. Kissel, S. Klimenko, K. Kokeyama, V. Kondrashov, R. Kopparapu, S. Koranda, D. Kozak, B. Krishnan, R. Kumar, P. Kwee, P. K. Lam, M. Landry, B. Lantz, A. Lazzarini, H. Lei, M. Lei, N. Leindecker, I. Leonor, C. Li, H. Lin, P. E. Lindquist, T. B. Littenberg, N. A. Lockerbie, D. Lodhia, M. Longo, M. Lormand, P. Lu, M. Lubinski, A. Lucianetti, H. Lück, B. Machenschalk, M. MacInnis, M. Mageswaran, K. Mailand, I. Mandel, V. Mandic, S. Márka, Z. Márka, A. Markosyan, J. Markowitz, E. Maros, I. W. Martin, R. M. Martin, J. N. Marx, K. Mason, F. Matichard, L. Matone, R. A. Matzner, N. Mavalvala, R. McCarthy, D. E. McClelland, S. C. McGuire, M. McHugh, G. McIntyre, D. J. A. McKechan, K. McKenzie, M. Mehmet, A. Melatos, A. C. Melissinos, D. F. Menéndez, G. Mendell, R. A. Mercer, S. Meshkov, C. Messenger, M. S. Meyer, J. Miller, J. Minelli, Y. Mino, V. P. Mitrofanov, G. Mitselmakher, R. Mittleman, O. Miyakawa, B. Moe, S. D. Mohanty, S. R. P. Mohapatra, G. Moreno, T. Morioka, K. Mors, K. Mossavi, C. MowLowry, G. Mueller, H. Müller-Ebhardt, D. Muhammad, S. Mukherjee, H. Mukhopadhyay, A. Mullavey, J. Munch, P. G. Murray, E. Myers, J. Myers, T. Nash, J. Nelson, G. Newton, A. Nishizawa, K. Numata, J. O'Dell, B. O'Reilly, R. O'Shaughnessy, E. Ochsner, G. H. Ogin, D. J. Ottaway, R. S. Ottens, H. Overmier, B. J. Owen, Y. Pan, C. Pankow, M. A. Papa, V. Parameshwaraiah, P. Patel, M. Pedraza, S. Penn, A. Perraca, V. Pierro, I. M. Pinto, M. Pitkin, H. J. Pletsch, M. V. Plissi, F. Postiglione,

M. Principe, R. Prix, L. Prokhorov, O. Punken, V. Quetschke, F. J. Raab, D. S. Rabeling, H. Radkins, P. Raffai, Z. Raics, N. Rainer, M. Rakhmanov, V. Raymond, C. M. Reed, T. Reed, H. Rehbein, S. Reid, D. H. Reitze, R. Riesen, K. Riles, B. Rivera, P. Roberts, N. A. Robertson, C. Robinson, E. L. Robinson, S. Roddy, C. Röver, J. Rollins, J. D. Romano, J. H. Romie, S. Rowan, A. Rüdiger, P. Russell, K. Ryan, S. Sakata, L. S. de la Jordana, V. Sandberg, V. Sannibale, L. Santamaría, S. Saraf, P. Sarin, B. S. Sathyaprakash, S. Sato, M. Satterthwaite, P. R. Saulson, R. Savage, P. Savov, M. Scanlan, R. Schilling, R. Schnabel, R. Schofield, B. Schulz, B. F. Schutz, P. Schwinberg, J. Scott, S. M. Scott, A. C. Searle, B. Sears, F. Seifert, D. Sellers, A. S. Sengupta, A. Sergeev, B. Shapiro, P. Shawhan, D. H. Shoemaker, A. Sibley, X. Siemens, D. Sigg, S. Sinha, A. M. Sintes, B. J. J. Slagmolen, J. Slutsky, J. R. Smith, M. R. Smith, N. D. Smith, K. Somiya, B. Sorazu, A. Stein, L. C. Stein, S. Steplewski, A. Stochino, R. Stone, K. A. Strain, S. Strigin, A. Stroeer, A. L. Stuver, T. Z. Summerscales, K.-X. Sun, M. Sung, P. J. Sutton, G. P. Szokoly, D. Talukder, L. Tang, D. B. Tanner, S. P. Tarabrin, J. R. Taylor, R. Taylor, J. Thacker, K. A. Thorne, A. Thüring, K. V. Tokmakov, C. Torres, C. Torrie, G. Traylor, M. Trias, D. Ugolini, J. Ulmen, K. Urbanek, H. Vahlbruch, M. Vallisneri, C. V. D. Broeck, M. V. van der Sluys, A. A. van Veggel, S. Vass, R. Vaulin, A. Vecchio, J. Veitch, P. Veitch, C. Veltkamp, A. Villar, C. Vorvick, S. P. Vyachanin, S. J. Waldman, L. Wallace, R. L. Ward, A. Weidner, M. Weinert, A. J. Weinstein, R. Weiss, L. Wen, S. Wen, K. Wette, J. T. Whelan, S. E. Whitcomb, B. F. Whiting, C. Wilkinson, P. A. Willems, H. R. Williams, L. Williams, B. Willke, I. Wilmut, L. Winkelmann, W. Winkler, C. C. Wipf, A. G. Wiseman, G. Woan, R. Wooley, J. Worden, W. Wu, I. Yakushin, H. Yamamoto, Z. Yan, S. Yoshida, M. Zanolin, J. Zhang, L. Zhang, C. Zhao, N. Zotov, M. E. Zucker, H. zur Mühlen, and J. Zweizig, "LIGO: the laser interferometer gravitational-wave observatory," *Reports on Progress in Physics*, vol. 72, p. 076901, jun 2009.

[8] N. T. Bishop, R. Gomez, L. Lehner, and J. Winicour, "Cauchy-characteristic extraction in numerical relativity," *Phys. Rev. D*, vol. 54, pp. 6153–6165, 1996, `arXiv:gr-qc/9705033`.

[9] R. Gomez, L. Lehner, P. Papadopoulos, and J. Winicour, "The eth formalism in numerical relativity," *Class. Quant. Grav.*, vol. 14, pp. 977–990, 1997, arXiv:gr-qc/9702002.

[10] N. T. Bishop, R. Gomez, L. Lehner, M. Maharaj, and J. Winicour, "High powered gravitational news," *Phys. Rev. D*, vol. 56, pp. 6298–6309, 1997, arXiv:gr-qc/9708065.

[11] J. Winicour, "Characteristic Evolution and Matching," *Living Reviews in Relativity*, vol. 1, no. 1, p. 5, 1998.

[12] J. Winicour, "Characteristic Evolution and Matching," *Living Rev. Rel.*, vol. 8, p. 10, 2005, arXiv:gr-qc/0508097.

[13] M. C. Babiuc, N. T. Bishop, B. Szilagyi, and J. Winicour, "Strategies for the Characteristic Extraction of Gravitational Waveforms," *Phys. Rev. D*, vol. 79, p. 084011, 2009, arXiv:0808.0861[gr-qc].

[14] M. C. Babiuc, B. Szilagyi, J. Winicour, and Y. Zlochower, "A Characteristic Extraction Tool for Gravitational Waveforms," *Phys. Rev. D*, vol. 84, p. 044057, 2011, arXiv:1011.4223[gr-qc].

[15] J. Winicour, "Characteristic Evolution and Matching," *Living Rev. Rel.*, vol. 15, no. 1, p. 2, 2012.

[16] J. Moxon, M. A. Scheel, S. A. Teukolsky, N. Deppe, N. Fischer, F. Hébert, L. E. Kidder, and W. Throwe, "SpECTRE Cauchy-characteristic evolution system for rapid, precise waveform extraction," *Phys. Rev. D*, vol. 107, no. 6, p. 064013, 2023, arXiv:2110.08635[gr-qc].

[17] T. Chu, H. Fong, P. Kumar, H. P. Pfeiffer, M. Boyle, D. A. Hemberger, L. E. Kidder, M. A. Scheel, and B. Szilagyi, "On the accuracy and precision of numerical waveforms: Effect of waveform extraction methodology," *Class. Quant. Grav.*, vol. 33, no. 16, p. 165001, 2016, arXiv:1512.06800[gr-qc].

[18] Y. Zlochower, M. Ponce, and C. O. Lousto, "Accuracy Issues for Numerical Waveforms," *Phys. Rev. D*, vol. 86, p. 104056, 2012, arXiv:1208.5494[gr-qc].

[19] J. R. Driscoll and D. M. Healy, "Computing Fourier Transforms and Convolutions on the 2-Sphere," *Adv. Appl. Math.*, vol. 15, no. 2, pp. 202–250, 1994.

[20] M. Fernando, D. Neilsen, Y. Zlochower, E. W. Hirschmann, and H. Sundar, "Massively parallel simulations of binary black holes with dendro-gr," 2022.